

quired, and prices are subject to change.

LITERATURE CITED

- (1) Jurs, P. C.; Sutton, G. P.; Ranc, M. L. *Anal. Chem.* **1989**, *61*, 1115A-1122A.
- (2) Fürst, A.; Pretsch, E. *Anal. Chim. Acta* **1990**, *229*, 17-25.
- (3) Sutton, G. P.; Anker, L. S.; Jurs, P. C. *Anal. Chem.* **1991**, *63*, 443-449.
- (4) Lindeman, L. P.; Adams, J. Q. *Anal. Chem.* **1971**, *43*, 1245-1252.
- (5) Smith, D. H.; Jurs, P. C. *J. Am. Chem. Soc.* **1978**, *100*, 3316-3321.
- (6) Small, G. W.; Jurs, P. C. *Anal. Chem.* **1983**, *55*, 1128-1134.
- (7) Small, G. W.; Jurs, P. C. *Anal. Chem.* **1984**, *56*, 2307-2314.
- (8) Egoif, D. S.; Jurs, P. C. *Anal. Chem.* **1987**, *59*, 1586-1593.
- (9) Egoif, D. S.; Brockett, E. B.; Jurs, P. C. *Anal. Chem.* **1988**, *60*, 2700-2706.
- (10) Sutton, G. P.; Jurs, P. C. *Anal. Chem.* **1989**, *61*, 863-871.
- (11) Ranc, M. L.; Jurs, P. C. *Anal. Chem.* **1989**, *61*, 2489-2496.
- (12) Egoif, D. S.; Jurs, P. C. *Anal. Chem.* **1990**, *62*, 1746-1754.
- (13) Sutton, G. P.; Jurs, P. C. *Anal. Chem.* **1990**, *62*, 1884-1891.
- (14) Ranc, M. L.; Jurs, P. C. *Anal. Chim. Acta*, **1991**, *248*, 183-193.
- (15) Small, G. W.; Jurs, P. C. *Anal. Chem.* **1984**, *56*, 2314-2319.
- (16) Small, G. W.; Jurs, P. C. *Anal. Chem.* **1984**, *56*, 1314-1323.
- (17) Stothers, J. B.; Tan, C. T. *Can. J. Chem.* **1974**, *308*, 308-314.
- (18) Heathcock, C. H.; Germroth, T. C.; Graham, S. L. *J. Org. Chem.* **1979**, *44*, 4481-4487.
- (19) Christl, M.; Roberts, J. D. *J. Org. Chem.* **1972**, *37*, 3443-3452.
- (20) Brugger, W. E.; Jurs, P. C. *Anal. Chem.* **1975**, *47*, 781-783.
- (21) Stuper, A. J.; Jurs, P. C. *J. Chem. Inf. Comput. Sci.* **1976**, *16*, 99-105.
- (22) Rohrbach, R. H.; Jurs, P. C. UDRAW. Quantum Chemistry Exchange, Program 300; Indiana University: Bloomington, IN, 1988.
- (23) Stuper, A. J.; Brugger, W. E.; Jurs, P. C. *Computer Assisted Studies of Chemical Structure and Biological Function*; Wiley-Interscience: New York, 1979; pp 83-90.
- (24) Burkert, U.; Allinger, N. L. *Molecular Mechanics*; ACS Monograph 177; American Chemical Society: Washington, DC, 1982.
- (25) Clark, T. *A Handbook of Computational Chemistry: A Practical Guide to Chemical Structure and Energy Calculations*; Wiley: New York, 1985; Chapters 1 and 2.
- (26) Tou, J. T.; Gonzalez, R. C. *Pattern Recognition Principles*; Addison-Wesley: Reading, MA, 1974; pp 271-283.
- (27) Eilert, E. L.; Allinger, N. L.; Angyal, S. J.; Morrison, G. A. *Conformational Analysis*; Wiley-Interscience: New York, 1965; pp 201-211.
- (28) St-Jacques, M.; Vaziri, C.; Frenette, D. A.; Goursot, A.; Fliszá, S. J. *Am. Chem. Soc.* **1976**, *98*, 5759-5765.
- (29) Randić, M. *J. Chem. Inf. Comput. Sci.* **1984**, *24*, 164-175.

RECEIVED for review July 1, 1991. Accepted August 8, 1991. This work was supported by the National Science Foundation (Grant CHE-8815785) and by the Department of Defense (Grant DAAL03-89-G-0069). The Sun 4/110 Workstation was purchased with partial financial support of the National Science Foundation. Portions of this paper were presented at the 201st National Meeting of the American Chemical Society, Atlanta, GA, April 1991.

Scanning Electrochemical Microscopy. 11. Improvement of Image Resolution by Digital Processing Techniques

Chongmok Lee,¹ David O. Wipf, and Allen J. Bard*

Department of Chemistry and Biochemistry, The University of Texas at Austin, Austin, Texas 78712

Keith Bartels and Alan C. Bovik

Department of Electrical and Computer Engineering, The University of Texas at Austin, Austin, Texas 78712

Images obtained by scanning electrochemical microscopy (SECM) were improved (deblurred) by use of digital image processing techniques, i.e., a linear combination of Laplacian and Gaussian filtering. Image improvement of repetitive structure (minigrids; interdigitated arrays) and an irregular structure (the bottom surface of a *Ligustrum sinense* leaf) is described.

INTRODUCTION

In the last decade, microscopes other than conventional microscopes (e.g., light or electron microscopes that are based on the use of electromagnetic radiation) have been devised by scanning a small tip on or near the surface of interest. For example, the scanning tunneling microscope (STM) (1) has led to several variants, such as the atomic force microscope (AFM) (2) and the ion-conductance microscope (3).

In scanning electrochemical microscopy (SECM), a microvoltammeter tip electrode (with a microdisk geometry and a tip radius of 0.1-12.5 μm) is rastered in close proximity to the substrate to be imaged in a solution containing an electroactive species (4-6). Previous reports from this laboratory described imaging of surfaces by employing the feedback

mode, where the steady-state tip current, i_T , controlled by an electrochemical reaction at the tip electrode, is a function of the solution composition, tip-substrate distance, d , and the nature of the substrate itself. The measurement of i_T can thus provide information about the topography of the sample surface as well as its electrical and chemical properties; electrodes (e.g., minigrids and interdigitated electrode arrays) (6-8), polymer and oxide films on electrode (7, 9), and biological materials (10) have been imaged. Thus SECM allows, at least in favorable circumstances, analysis of surface features with high spatial resolution. Other groups have used a microdisk electrode to monitor a substance generated at the substrate (11, 12) or a hemispherical microelectrode to measure the local flux of electroactive ions across a porous membrane (13).

Resolution in SECM depends upon the perturbation of the tip current by substrate features and is controlled by the size and shape of the tip electrode and the ability to bring it into close proximity with the substrate surface ($d < 4a$, where a is the radius of a tip) (14). Submicron resolution in SECM has been demonstrated using a tip electrode with a diameter of 0.2 μm (8). This paper deals with the improvement of resolution in SECM by the application of image processing techniques. Such techniques have been applied in a number of areas since its early use in restoring the transmitted moon images in the early 1960s (15, 16). This study demonstrates that the resolution of the SECM images can be substantially

¹Current address: Division of Chemistry and Chemical Engineering, California Institute of Technology, Pasadena, CA 91125.

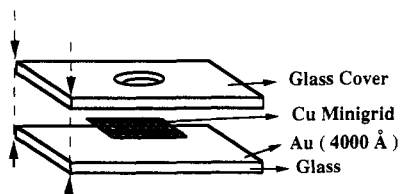


Figure 1. Schematic diagram of the preparation of the inverse indium tin oxide (ITO) grid structure.

improved using this technique. Improvement of the image is shown qualitatively by comparing the raw image with that of the image after processing or that using a smaller tip electrode.

EXPERIMENTAL SECTION

Apparatus and Materials. Instrumental details and operational procedures for the SECM were described previously (6). Milli-Q reagent water (Millipore) was used to prepare aqueous solutions of $K_4Fe(CN)_6$, $Ru(NH_3)_6Cl_3$, K_2SO_4 , KCl , H_2SO_4 , and phosphate-citrate (McIlvaine) buffers. All chemicals were of reagent grade and were used as received. A carbon-microdisk electrode tip (radius $5.5 \mu m$) and a platinum-microdisk electrode tip (radius $1 \mu m$) were fabricated as described (4). Image-processing calculations were performed on a Sun 3/260 work station and an IBM PC compatible 386 computer.

Preparation of Substrates. A schematic diagram of the method of preparation of the inverse indium tin oxide (ITO) grid structure is illustrated in Figure 1. A piece ($1 cm \times 1 cm$) of Cu minigrad screen ($25 \mu m$ periodicity; Ted Pella, Inc., Redding, CA) was placed on a Au film (ca. $400 nm$ thick) that was sputtered on a glass slide. A second glass slide, with a circular hole ($2\text{-}mm$ diameter), was clamped over the Cu minigrad screen. The ITO structure was formed by sputtering about a $20\text{-}nm$ -thick layer of ITO over the screen. This leaves a structure consisting of ITO mounds separated by a less conductive inverse replica of the minigrad. The previously obtained SECM image of the lower surface of a *Ligustrum sinense* leaf (10) was used as another sample to test our program. Pb/Cu sandwich electrodes were constructed by interleaving sheets of $50\text{-}\mu m$ -thick Pb and $18\text{-}\mu m$ -thick Cu foil. The interleaved sheets were compressed and potted in EPON 828 epoxy (Shell Chemical Co., Houston, TX). The epoxy/foil assembly was ground and polished to expose the foil edges. Before use, the Pb/Cu sandwich electrode was polished with $0.05\text{-}\mu m$ alumina. All the Pb and Cu foil sheets were in electrical contact. The interdigitated electrode array (IDA) electrode was a generous gift from Melani Sullivan, University of North Carolina at Chapel Hill. The IDA consists of $3\text{-}\mu m$ -wide platinum bands spaced by $5\text{-}\mu m$ widths of silicon dioxide insulator.

THEORY

Image-processing techniques (15, 16) are widely used in scanning tunneling microscopy. Generally, these involve treatment of the image by low- or high-pass filters, or Fourier transformation followed by attenuation of certain frequencies and inverse transformation. Since image formation in SECM depends upon electrochemical processes at features, the process which causes blurring is a diffusional one. Thus the approach taken here was to restore (deblur) the image by considering the diffusion process, i.e., using an analogue of Fick's law, eq 1, where $g(x,y,t)$ is the two-dimensional image,

$$\nabla^2 g(x,y,t) = \frac{\partial}{\partial t} g(x,y,t) \quad (1)$$

t is a function of time, and ∇ is the Laplacian operator. $g(x,y,\tau)$, where $\tau > 0$, is the experimentally obtained image and $g(x,y,0)$ is the desired deblurred image. The tip current, in the usual SECM experiment is a steady-state current. However, time must be considered as a parameter, since it is related to the tip-substrate distance, d , through the diffusion equation ($t \approx d^2/2D$). In other words, the blurring of the steady-state image represents how far (over a time t) mediator diffuses

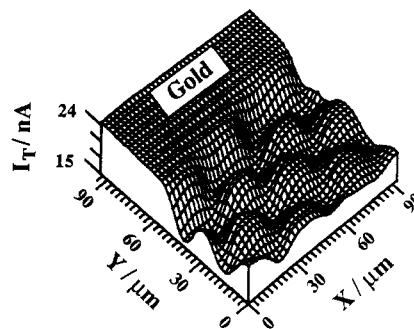


Figure 2. SECM scan of the boundary between Au layer (left) and inverse grid structure (right). The potential of the tip electrode, E_T , was held at $-0.38 V$ vs SCE in an aqueous solution containing $15 mM Ru(NH_3)_6Cl_3$ and $50 mM K_2SO_4$ with a C-microdisk tip electrode (radius $5.5 \mu m$). $I_{T,\infty} \approx 15 nA$.

from a feature on the substrate. If we expand $g(x,y,t)$ at $t = \tau$ using a Taylor series and truncate the second and higher order terms, we obtain

$$g(x,y,t) = g(x,y,\tau) + (t - \tau) \left[\frac{\partial}{\partial t} g(x,y,t) \right]_{t=\tau} \quad (2)$$

Substituting eq 1 into eq 2 and letting $t = 0$, yields

$$g(x,y,0) \approx g(x,y,\tau) - \tau \nabla^2 g(x,y,\tau) \quad (3)$$

Equation 3 implies that an approximation to the deblurred image can be found by subtracting a constant multiple of the Laplacian of the obtained image from that image. This technique is commonly known as *unsharp masking* (16).

However, SECM images contain high-frequency noise and the parabolic frequency response of the Laplacian operator enhances this noise. The noise from the Laplacian operator can be reduced by low-pass filtering of the output with a Gaussian filter. The Gaussian filter is chosen because of its optimal balance between spatial and spectral localization. The linear combination of Laplacian and Gaussian filtering, which is a band-pass filter, is the Laplacian of Gaussian (LOG) filter often used in edge detection algorithms (17). The LOG filter, $l(x,y)$, has the form

$$l(x,y) = \frac{-1}{\pi\sigma^4} \left(1 - \frac{x^2 + y^2}{2\sigma^2} \right) \exp \left[\frac{-(x^2 + y^2)}{2\sigma^2} \right] \quad (4)$$

Therefore, our restoration equation becomes

$$g(x,y,0) = g(x,y,\tau) - \tau l(x,y) * g(x,y,\tau) \quad (5)$$

where $*$ represents the convolution operation. This is implemented by the algorithm

$$\hat{g}(i,j) = g(i,j) - \tau \sum_a \sum_b g(i-a, j-b) l(a,b) \quad (6)$$

where (i,j) are discrete image coordinates, $g(i,j)$ is the recorded image, $\hat{g}(i,j)$ is the restored (deblurred) image, $l(a,b)$ is the LOG operator, eq 4, and a and b are taken from $(-n+1)/2$ to $(n-1)/2$; the parameters $n \approx 8\sigma$ and τ are adjustable. In this work τ was taken as 5.0 or 10.0 and σ as 1.0, so that $n = 9$; $l(a,b)$ was thus a 9×9 matrix indexed $(-4, -3, \dots, 3, 4)$. Further details of this approach and choice of parameters, and a comparison of restoration by inverse filtering are described elsewhere (18). By empirically choosing values for τ and σ we have improved the SECM images of either repetitive (e.g., minigrad structures or an IDA electrode) or irregular structures (e.g., the bottom surface of a *L. sinense* leaf or a Pb/Cu sandwich electrode).

RESULTS AND DISCUSSION

Inverse ITO Minigrad. The conductive nature of the sample surface was probed by SECM x - y scans above the

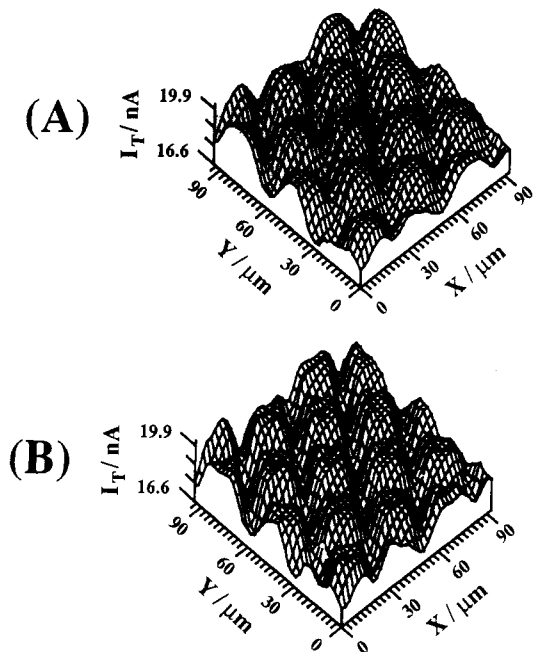


Figure 3. (A) Three-dimensional view of SECM scan of the inverse grid structure. Experimental conditions were the same as in Figure 2. (B) Three-dimensional view of (A) after application of the restoration algorithm (eq 6).

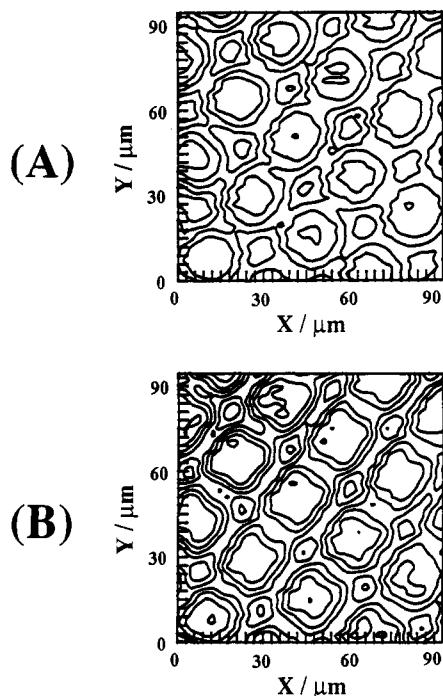


Figure 4. I_T contour map of Figure 3: (A) raw experimental result; (B) after application of the restoration algorithm (eq 6).

region at the boundary between the Au film and the ITO grid structures (Figure 2). The aqueous solution in which this sample was immersed contained 15 mM $Ru(NH_3)_6Cl_3$ and 50 mM K_2SO_4 . The microdisk tip electrode (C; radius 5.5 μm) was held at -0.38 V vs SCE where the reduction of $Ru(NH_3)_6^{3+}$ to $Ru(NH_3)_6^{2+}$ occurs. As the SECM response depends upon surface conductivity, a positive feedback was observed ($i_T > i_{T,\infty}$, where $i_{T,\infty}$ is the tip current when the tip is held far from the substrate; $i_{T,\infty}$ was ca. 15 nA in Figure 2) when the tip was over the Au layer because of regeneration of $Ru(NH_3)_6^{3+}$ at the substrate. A similar amount of positive feedback current was also observed above the region where the holes of the Cu minigrad were located, in which 20-nm-thick ITO mounds over

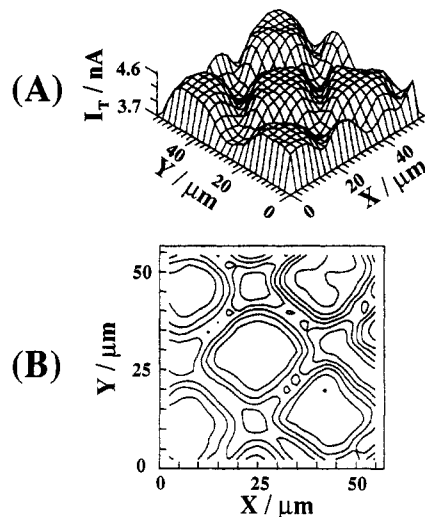


Figure 5. SECM scan of the inverse grid structure with a Pt-microdisk tip electrode (radius 1 μm). The solution and E_T were the same as in Figure 2: (A) three-dimensional view; (B) I_T contour map.

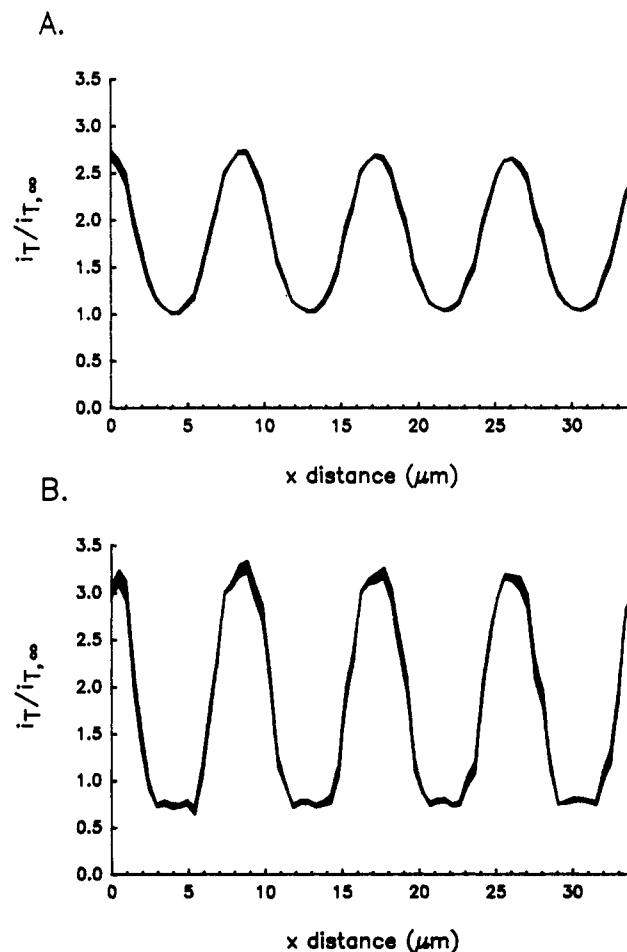


Figure 6. Cross-sectional view of the SECM line scan over the $3 \times 5 \mu m$ IDA electrode. Tip is a 1- μm -radius Pt disk held at a potential of -0.32 V vs Ag/AgCl. Mediator solution is 2.0 mM $Ru(NH_3)_6^{3+}$ in pH 4.0 buffer: (A) unfiltered scan at a tip-substrate separation, d , of 0.4 μm ; (B) LOG filtered data from (A) for $\tau = 5$, $\sigma = 1$.

the Au film were produced. A much smaller positive feedback current was observed above the region where the lines of Cu minigrad were located (Figure 2). The reason for the decreased rate of oxidation of Ru(II) in the region shadowed by the Cu minigrad is not clear but is an example of differential surface reactivity imaging caused by differences in heterogeneous

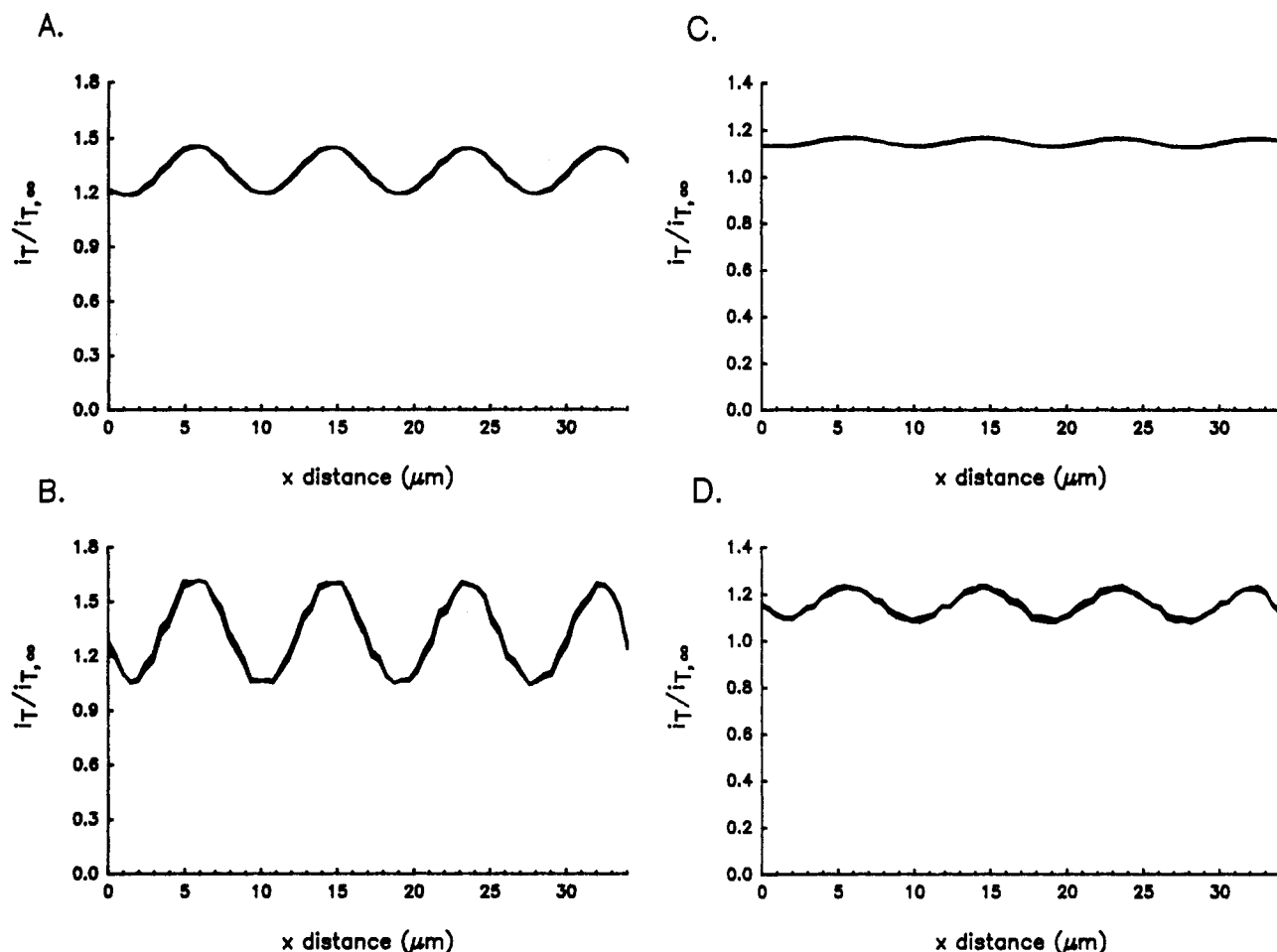


Figure 7. Cross-sectional view of SECM line scan over the $3 \times 5 \mu\text{m}$ IDA electrode. Conditions are the same as in Figure 6: (A) unfiltered scan at $d = 1.4 \mu\text{m}$; (B) restored image from (A) for $\tau = 10$, $\sigma = 1$; (C) unfiltered scan at $d = 3.3 \mu\text{m}$, (D) LOG filtered data from (C) for $\tau = 25$, $\sigma = 1$.

electron-transfer rates (7, 19, 20). Overall, the SECM scan of this sample is the inverse of that of a Au minigrad shown earlier (6). Note that this SECM scan shows a surface conductivity map of the sample rather than the actual surface topography.

To show the effect of image processing, the raw image of the grid structure (Figure 3A) is compared to one processed via the restoration algorithm (eq 6) (Figure 3B). The three-dimensional views of the SECM images were converted to the current contour maps (Figure 4), where improvement of edge detection is clear. For comparison of the improvement of the SECM resolution by this image-processing technique with that obtained by the use of a smaller tip electrode, an SECM scan of the same substrate with a Pt-microdisk tip electrode (radius $1 \mu\text{m}$) is shown in Figure 5. Although the resolution of Figure 4B is not as good as that in Figure 5B, the original SECM image (Figure 4A) is improved to be equivalent to one obtained with a tip 3–4 times smaller using the image-processing technique.

Platinum IDA Electrode. The substrate here is an interdigitated array (IDA) of electrodes with $3\text{-}\mu\text{m}$ -wide Pt bands separated by a $5\text{-}\mu\text{m}$ -wide SiO_2 insulator. The thickness of the Pt bands is about $0.15 \mu\text{m}$. A cross-sectional view of a SECM scan over the IDA is shown in Figure 6A. The image was produced with a Pt tip electrode in a solution of $2.0 \text{ mM Ru}(\text{NH}_3)_6^{3+}$ in pH 4.0 buffer at a tip-substrate separation of $0.4 \mu\text{m}$. Although the IDA periodicity of $3 \times 5 \mu\text{m}$ is clearly seen, the band structure remains incompletely resolved. After application of the LOG-based filter technique (eq 6), ($\tau = 5$, $\sigma = 1$) to the image in Figure 6A, an improvement in the resolution is observed. Note, however, that the sides of the

band structure are still sloped. This demonstrates that the ultimate resolution achievable is limited by the size of the imaging tip itself. In this case, the tip is $2 \mu\text{m}$ in diameter and, thus, gives about a $2\text{-}\mu\text{m}$ resolution on the image.

The ability of the restoration algorithm (eq 6) to resolve more diffusively blurred images was tested by scanning over the IDA electrode with greater tip-substrate distance, d . Figure 7A shows a cross-sectional image taken at $d = 1.4 \mu\text{m}$; because of the greater separation, the diffusional blurring is large. The nominal periodicity of the IDA is preserved in the image, but the structure is unresolved. Application of eq 6 ($\tau = 10$, $\sigma = 1$) improves the resolution slightly but at the cost of decreased signal to noise ratio. Here, the restoration algorithm was unable to remove adequately the diffusional blurring without a simultaneous increase in spurious noise.

Copper/Lead Sandwich Composite. The SECM was used to image a substrate constructed of $50\text{-}\mu\text{m}$ -thick Pb foil sheets interleaved with $18\text{-}\mu\text{m}$ -thick Cu foil. Upon immersion of the sandwich structure in a solution of $2.6 \text{ mM Ru}(\text{NH}_3)_6^{3+}$ and $0.5 \text{ M H}_2\text{SO}_4$, the exposed Pb edge was passivated (presumably by formation of PbSO_4) while the $\text{Ru}(\text{NH}_3)_6^{3+}$ was reduced to $\text{Ru}(\text{NH}_3)_6^{2+}$. An image of the surface was made with a $1\text{-}\mu\text{m}$ -radius Pt tip held at an oxidizing potential to regenerate $\text{Ru}(\text{NH}_3)_6^{3+}$. The gray-scale image of the surface (Figure 8A) clearly shows a band structure corresponding to the foil edges. Note that this image was preprocessed to remove the scan line-to-scan line variation in the baseline value. A positive feedback signal is observed at the active Cu regions, while the passive Pb produces negative feedback. An improvement in the SECM image is obtained by use of the restoration algorithm (eq 6) ($\tau = 5$, $\sigma = 1$) on the image in

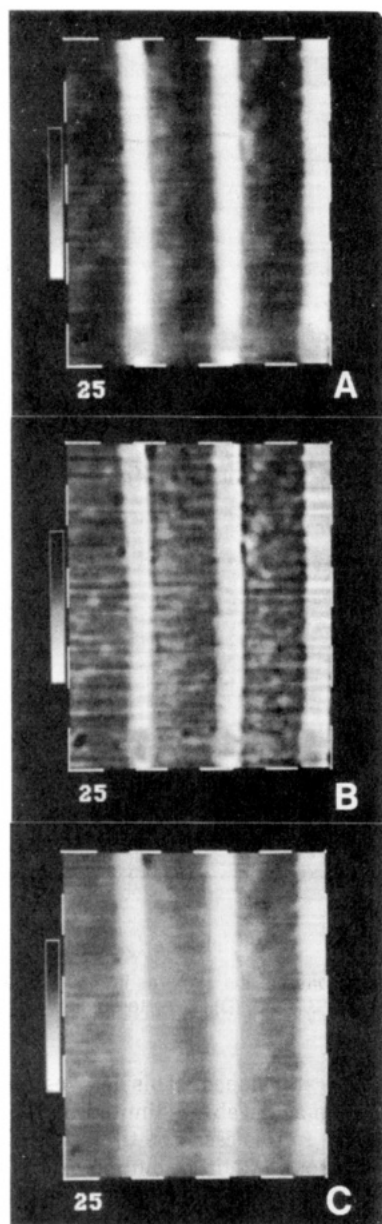


Figure 8. Gray-scaled SECM scan of a $200 \times 200 \mu\text{m}$ section of the Cu/Pb sandwich structure in a 2.6 mM solution of $\text{Ru}(\text{NH}_3)_6^{3+}$ in 0.5 M H_2SO_4 at a $1\text{-}\mu\text{m}$ -radius Pt-disk electrode. Tip potential, E_T , was held at +0.3 V vs Ag/AgCl. The substrate was not potentiostated and was poised at a potential of about -0.25 V: (A) unfiltered data, current range = 2.45–3.0 nA; (B) restored image ($\tau = 5$, $\sigma = 1$), current range = 2.2–3.2 nA; (C) unfiltered data at the same contrast level as the restored data, current range = 2.2–3.2 nA.

Figure 8A, yielding Figure 8B. As in Figure 2, a significant improvement in edge resolution is seen, as well as improvement in the resolution of other features such as the pitlike structures observed at various places in the PbSO_4 layer. Moreover, a depression running parallel to the Cu/Pb boundary can now be observed. This depression could be due to the thin insulating layer of epoxy joining the two materials. However, an artifact due to the filtering process is not yet ruled out.

Bottom Surface of a *L. sinense* leaf. To check the generality of this technique, we used it on the SECM image of the irregular structure on an insulating substrate, the bottom surface of a *L. sinense* leaf (10). Figure 9A is the SECM image obtained with a Pt-microdisk (radius $1 \mu\text{m}$) electrode, where the variation of i_T was converted to produce a gray-scale presentation; dark color, maximum current; light color, minimum current. The better resolution in Figure 9B

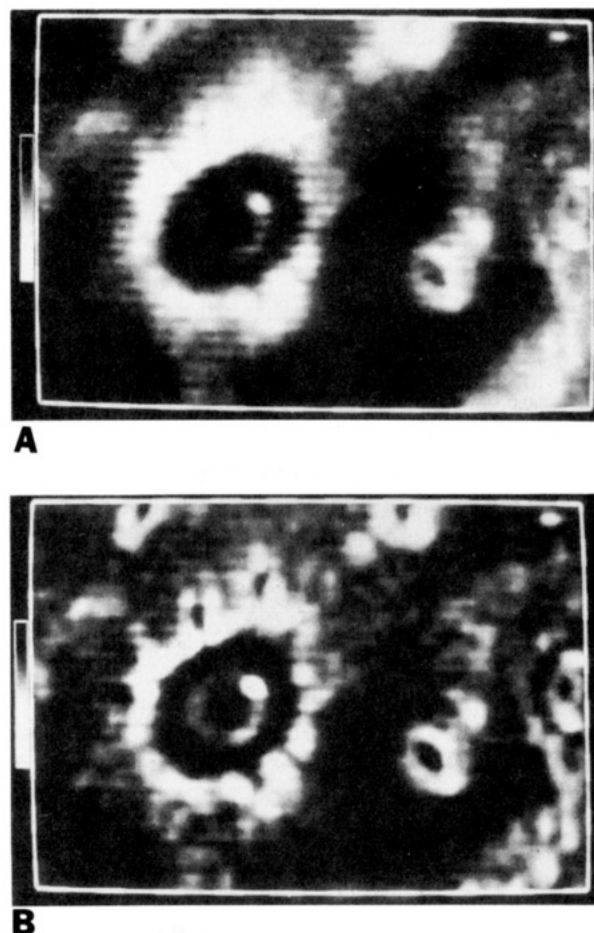


Figure 9. Gray-scaled image of the bottom surface of a *L. sinense* leaf in a 20 mM $\text{K}_4\text{Fe}(\text{CN})_6$ and 0.1 M KCl solution scanned with a $1\text{-}\mu\text{m}$ -radius Pt tip: scan area, $188 \times 142 \mu\text{m}$; $0.73 \text{ nA} < i_T < 2.75 \text{ nA}$. Here the dark shades represent maximum i_T and larger d , and light shades, minimum i_T and smaller d : (A) raw experimental data; (B) restored image.

was obtained by use of eq 6, where a large craterlike feature at middle-left showed finer structure and some stomata at the upper-right and middle-right edges showed their structures more clearly.

CONCLUSIONS

The application of image-processing techniques involving a combination of Laplacian and Gaussian filtering improves the resolution of experimentally obtained SECM images for conductive or insulating structures of various types. A combination of this filtering technique and smaller tip electrodes should bring the resolution of SECM to the $100\text{-}\text{\AA}$ level. However, our best resolution at this time was obtained with tips with a $0.1\text{-}\mu\text{m}$ radius (8). For higher resolution, smaller metal tips surrounded by insulators, such as those described for use in STM for samples immersed in liquids (21, 22) might be useful in SECM. Such very high resolution SECM will require more precise micropositioning devices and greater attention to the minimization of thermal drift and vibrations. Moreover, the application of small tips will involve very close (\sim tip radius, a) spacings between tip and substrate, which implies that a constant current feedback mode, such as that frequently employed in STM, will be more appropriate. This becomes especially challenging for imaging of surfaces showing both insulating and conductive regions. These aspects of SECM are currently under investigation in this laboratory.

ACKNOWLEDGMENT

We appreciate the assistance of D. Mandler in the preparation of the ITO sample substrates.

LITERATURE CITED

- (1) Binnig, G.; Rohrer, H. *Helv. Phys. Acta* **1982**, *55*, 726.
- (2) Binnig, G.; Quate, C.; Gerber, C. *Phys. Rev. Lett.* **1986**, *56*, 930.
- (3) Hansma, P. K.; Drake, B.; Marti, O.; Gould, S. N. C.; Prater, C. B. *Science* **1989**, *243*, 641 and references therein to other types of scanning microscopes.
- (4) Bard, A. J.; Fan, F.-R. F.; Kwak, J.; Lev, O. *Anal. Chem.* **1989**, *61*, 132.
- (5) Bard, A. J.; Denuault, G.; Lee, C.; Mandler, D.; Wipf, D. O. *Acc. Chem. Res.* **1990**, *23*, 357.
- (6) Kwak, J.; Bard, A. J. *Anal. Chem.* **1989**, *61*, 1794.
- (7) Lee, C.; Bard, A. J. *Anal. Chem.* **1990**, *62*, 1906.
- (8) Lee, C.; Miller, C. J.; Bard, A. J. *Anal. Chem.* **1991**, *63*, 78.
- (9) Kwak, J.; Lee, C.; Bard, A. J. *J. Electrochem. Soc.* **1990**, *137*, 1481.
- (10) Lee, C.; Kwak, J.; Bard, A. J. *Proc. Natl. Acad. Sci. U.S.A.* **1990**, *87*, 1740.
- (11) Engstrom, R. C.; Meaney, T.; Tople, R.; Wightman, R. M. *Anal. Chem.* **1987**, *59*, 2005.
- (12) Engstrom, R. C.; Weber, M.; Wunder, D. J.; Burgess, R.; Winquist, S. *Anal. Chem.* **1988**, *58*, 844.
- (13) Scott, E. R.; White, H. S.; Phipps, J. B. *J. Membr. Sci.* **1991**, *58*, 71.
- (14) Kwak, J.; Bard, A. J. *Anal. Chem.* **1989**, *61*, 1221.
- (15) Andrews, H. C.; Hunt, B. R. *Digital Image Restoration*; Prentice-Hall: Englewood Cliffs, NJ, 1977.
- (16) Rosenfeld, A.; Kak, A. C. *Digital Picture Processing*, 2nd Ed.; Academic Press: New York, 1982; Vol. 1.
- (17) Marr, D. *Vision*; W. H. Freeman and Co.: New York, 1982.
- (18) Bartels, K.; Bovik, A. C.; Lee, C.; Bard, A. J. Proceedings of the SPIE/SPSE Symposium on Electronic Imaging Science and Technology, San Jose, California, Feb 24 to March 1, 1991.
- (19) Wipf, D. O.; Bard, A. J. *J. Electrochem. Soc.* **1991**, *138*, 469.
- (20) Wipf, D. O.; Bard, A. J. *J. Electrochem. Soc.* **1991**, *138*, L4.
- (21) Gewirth, A. A.; Craston, D. H.; Bard, A. J. *J. Electroanal. Chem. Interfacial. Electrochem.* **1989**, *61*, 1630.
- (22) Penner, R. M.; Heben, M. J.; Lewis, N. S. *Anal. Chem.* **1989**, *61*, 1630.

RECEIVED for review May 20, 1991. Accepted August 12, 1991. We gratefully acknowledge the support of the study by the National Science Foundation (Grant CHE8901450) and the Texas Advanced Research Program.

Quantitative Surface Analysis of Organic Polymer Blends Using a Time-of-Flight Static Secondary Ion Mass Spectrometer

Patrick M. Thompson

Surface Science Section, Research Laboratories, Eastman Kodak Company, Rochester, New York 14650-2132

The surface composition of organic polymer blends can be determined using X-ray photoelectron spectroscopy (XPS) provided that each component in the blend has a unique element or functional group present. However, for blends not amenable to XPS, a relatively new technique with greater molecular specificity called static secondary ion mass spectrometry (SSIMS) holds the potential for determining the degree of surface segregation. Although SSIMS is generally considered to be a semiquantitative technique at best, arguments will be presented along with results showing that energy-focusing time-of-flight (TOF) mass spectrometers can overcome some of the possible instrumental artifacts associated with polymer surface analysis done by quadrupole SSIMS and that the SIMS matrix effect is not necessarily a major problem when organic polymer blends are analyzed. In this study, the surface compositions of an immiscible and a miscible polycarbonate/polystyrene blend were determined by TOF SIMS and XPS and these results were compared. The results for these two blends suggest that the accuracy for both TOF SSIMS and XPS can be within ± 0.1 monomer fraction, while the typical precision of the TOF SSIMS results were primarily determined by counting statistics and were generally better than those from XPS.

INTRODUCTION

The application of static secondary ion mass spectrometry (SSIMS) toward the qualitative analysis of inorganic and organic surfaces has been well documented (1-6). Success has been achieved with SSIMS as a semiquantitative or quantitative technique for organic surface analysis when calibrated by an independent technique such as X-ray photoelectron spectroscopy (7, 8).

Briggs et al. have shown that SSIMS alone can do semiquantitative if not quantitative surface analysis on random

copolymers of ethyl methacrylate/hydroxyethyl methacrylate, thus showing the potential for its use on other random copolymers (9). In random copolymers the surface composition should be similar to that of the bulk, therefore only a set of known bulk composition standards would be required to calibrate the SSIMS results.

In a study reported by Bhatia et al., XPS was used to calibrate static SIMS measurements made on a miscible blend of polystyrene and poly(vinyl methyl ether) (10). In that paper a sensitivity factor was calculated using XPS results which related the molar concentration of constituents to appropriate ion intensity ratios. This sensitivity factor was assumed to be independent of blend composition. These results suggested that matrix effects may be negligible in certain cases of miscible polymer blends.

In this paper a quantitative analysis scheme is proposed which uses the advantages of an energy-focusing time-of-flight mass spectrometer for determining the surface composition of miscible and immiscible organic polymer blends without necessarily requiring calibration by other surface-sensitive techniques. Similarly to Bhatia et al., this analysis scheme assumes that matrix effects are independent of the blend composition (10). In this paper some consideration is given to how matrix effects can effect the observed results depending on the type of instrument used and why they may be relatively independent of organic polymer blend composition.

Most methods proposed for SSIMS semiquantification and quantification involve comparisons of intensities of appropriately selected mass peaks, usually through a procedure involving their relative peak intensities (RPIs). In the simplest case, such as a two-component polymer blend, a RPI could be obtained between two different mass peaks, each primarily composed of a fragment ion or ions of the same nominal mass that uniquely represent one of the two polymers. By production of a series of blend compositions, a plot of the bulk composition versus RPI could be made. This plot would have